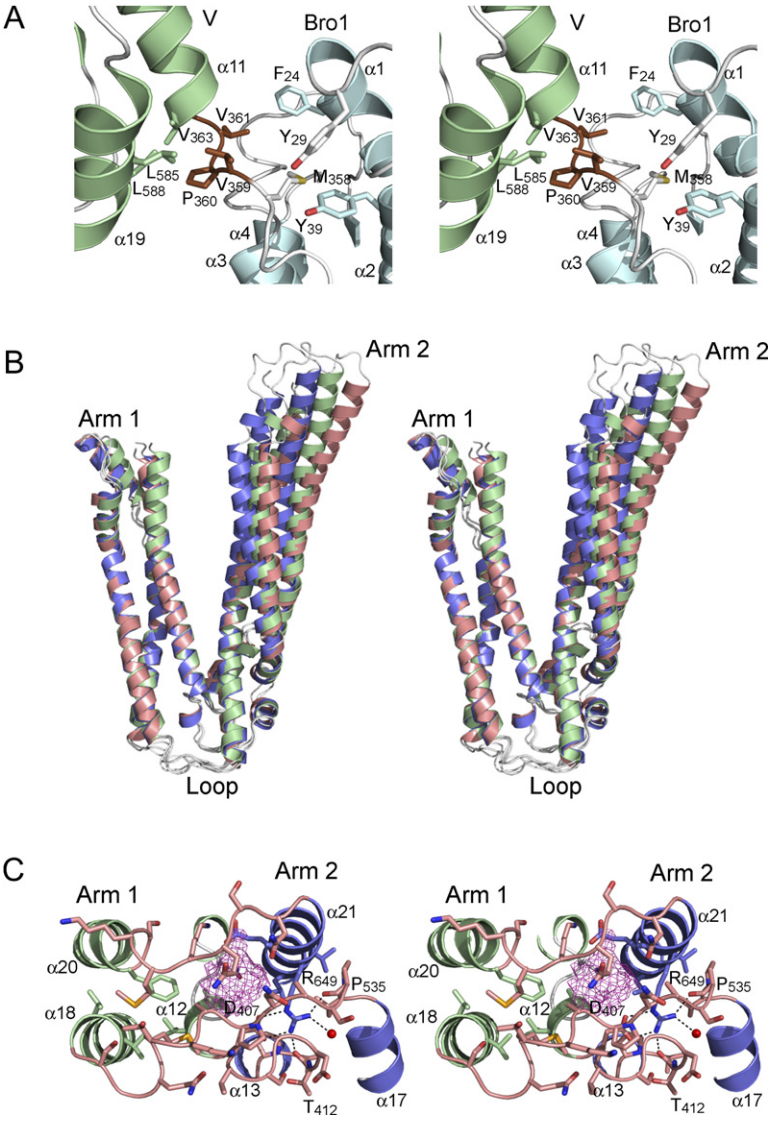

Figure 2. Interdomain Linkers and Conformational Flexibility of $ALIX_{Bro1-V}$

(A) Stereoview showing the linker between the Bro1 and V domains is shown. Secondary structures are color coded as in Figure 1B, and residues that contact the $_{359}VPV_{361}$ linker are shown explicitly.

(B) This stereoview illustrates conformational variability in different V-domain structures. The different trajectories of arm2 were visualized by superimposing only the arm1 regions from crystals of $ALIX_{Bro1-V}$ (salmon) and from the two different molecules in the $ALIX_V$ asymmetric unit (green and blue). The only other significant difference between the structures was in the position of Trp476 residue (α4/5 loop), which flips out of the core of arm2 in one of the two $ALIX_V$ structures to make a crystal contact.

(C) shows a stereoview illustrating the three-stranded loop region that connects the two arms of the V domain. Secondary structures are color coded as in Figure 1B. Side chains within the loop and adjacent residues are shown, and the stabilizing interactions of the Arg649 residue are shown explicitly. The purple cage denotes a pocket that appears to be occupied by a mix of ordered and disordered water molecules. The view is from the bottom of (B).

building the two helical bundles (Figure S3). Hence, the two arms are highly interconnected in primary sequence, and the entire V domain likely represents a single functional entity.

The two V-domain arms are primarily stabilized by hydrophobic side-chain-packing interactions that are based upon heptad repeats and that adopt canonical "knobs into holes" side-chain packing. This explains why the domain scored highly in coiled-coil prediction algorithms (Katoh et al., 2003; Odorizzi et al., 2003). In contrast, the three strands in the loops connecting arm1 and arm2 are stabilized almost exclusively by hydrophilic interactions, most of which are mediated by backbone atoms. An illustrative example is provided by the highly conserved Arg649 residue (α21, arm2), which forms a series of interactions that buttress the underside of the loop region; these include a buried salt bridge with Asp407 (α12/13 loop) and hydrogen-bonding interactions with a buried water molecule and with the backbone carbonyl oxygen atoms of Pro535 (α17/18 loop) and Thr412 (α12/13 loop). The loop region also encloses a hydrophilic interior cavity of ~67 $Å^3$ (purple in Figure 2C).

The V domain exhibits intrinsic conformational flexibility, as revealed by comparisons of the relative positions of the two arms in the different crystal structures. Isolated arm1 structures from the crystallographically independent models overlap well (rmsd = 1.4 Å), and the same is true for the arm2 structures, but overlapping on either arm causes the other to "fan out" into different positions. This is illustrated in Figure 2B for the case of overlap on arm1, where the relative arm2 displacements reach up to 10 Å at their distal ends. These global differences in the structures arise from small, cumulative changes in the interhelical packing interactions along both arms rather than from a dramatic reorganization of the loop region or elsewhere. Thus, the structures demonstrate that the V-domain arm